Highly crystalline ZnO film decorated with gold nanospheres for PIERS chemical sensing

Grégory Barbillon, Thomas Noblet, Christophe Humbert

PCCP
Physical Chemistry Chemical Physics

Accepted Manuscript

This article can be cited before page numbers have been issued, to do this please use: G. Barbillon, T. Noblet and C. HUMBERT, *Phys. Chem. Chem. Phys.*, 2020, DOI: 10.1039/D0CP03902K.

ROYAL SOCIETY OF CHEMISTRY

rsc.li/pccp

View Article Online
DOI: 10.1039/D0CP03902K

Journal Name

ARTICLE TYPE

Cite this: DOI: 00.0000/xxxxxxxxxx

Highly crystalline ZnO film decorated with gold nanospheres for PIERS chemical sensing

Grégory Barbillon,*[a] Thomas Noblet[b] and Christophe Humbert[b]

Received Date
Accepted Date

DOI: 00.0000/xxxxxxxxxx

In this paper, we report on the study of a novel type of substrate based on a highly crystalline ZnO film photo-irradiated by UV for enhancing Raman signal. This effect is called: photo-induced enhanced Raman spectroscopy (PIERS). This PIERS substrate is composed of a photo-irradiated thin ZnO film on which gold nanoparticles are deposited. This PIERS substrate allows to obtain large photo-induced SERS enhancement for the chemical detection of small molecules compared to normal SERS signal. This photo-induced SERS enhancement is due to increasing of electron density on the gold nanoparticles and charge transfer mechanisms. Here, we achieve a high quality PIERS substrate, whose signal exhibits weaker fluctuations and a similar or greater gain (up to 7.52) than those in current literature. Henceforth, these PIERS substrates are also easy to carry out for potential applications in industry.

In the last decade, the manufacturing of surface-enhanced Raman scattering (SERS) substrates with high enhancement factors and a low-cost of fabrication are key points for chemical and biological sensing [1,2]. On the one hand, a huge number of fabrication methods are available in order to obtain plasmonic nanostructures with different geometries such as chemical synthesis [3,4] and lithographic techniques [5,6]. Some of these various techniques are employed for their low-cost of fabrication: chemical synthesis, nanosphere lithography [7,8] (NSL) and nanoimprint lithography [5,9] (NIL). For NSL and NIL techniques, some limitations exist to obtain a good definition of plasmonic nanostructures on large surfaces required for practical applications of SERS substrates. On the other hand, the high enhancement factors come from both electromagnetic and chemical contributions. The most important contribution is the electromagnetic one (EM), which is dependent on and determined by the nanostructuring of the metallic surface [10]. The plasmonic nanostructures can confine the electromagnetic field at the nanoscale. Nevertheless, the design of the ideal SERS hotspots is difficult to achieve in terms of practicality and reproducibility. In addition, the chemical contribution is due to its microscopic origin such as the metal/molecule charge transfer resonance [11,12]. For both contributions, the molecules must be as close as possible to the metallic surface. First, EM enhancement indeed decreases exponentially with the distance from the surface [10]. Second, the charge transfer between the molecule and the substrate also depends on this distance [11]. In this paper, we report on a SERS enhancement obtained by UV-photo-irradiation of a highly crystalline ZnO film on which Au nanospheres are deposited. The use of a photo-irradiated semiconductor (here ZnO) film allows a strong Raman enhancement at the level of plasmonic nanoparticles beyond the normal SERS effect, so called in the whole text: photo-induced enhanced Raman scattering (PIERS). ZnO was chosen as a semiconductor for its wide direct band-gap (3.37 eV) in the near-UV spectral region [13]. Moreover, oxygen vacancies (V_O) in ZnO can be created under UV illumination, and behave as electron donors [13], which will be useful for PIERS effect. To the best of the authors' knowledge, no work demonstrated this effect with a highly crystalline ZnO film decorated by gold nanoparticles. The only demonstration of this PIERS effect from a ZnO film with Au nanoparticles was facing significant fluctuations of the signal due to a weak crystallinity [14]. Besides, a small number of research groups demonstrated this PIERS effect but based on a film or nanopore array of titanium dioxide covered by Au or Ag nanoparticles [15,16], or else based on aligned diphenylalanine peptide nanotubes covered with silver nanoparticles [17]. With our novel substrates, the chemical molecules will be adsorbed on plasmonic nanoparticles enabling a SERS enhancement by two potential contributions: electromagnetic and/or chemical [18–20].

In our paper, only the chemical contribution is investigated because the plasmon resonance of gold nanoparticles on the highly

[a] EPF-Ecole d'Ingénieurs, 3 bis rue Lakanal, 92330 Sceaux, France.
E-mail: gregory.barbillon@epf.fr
[b] Université Paris-Saclay, CNRS, Institut de Chimie Physique, UMR 8000, 91405 Orsay, France.

† Electronic Supplementary Information (ESI) available. See DOI: 00.0000/00000000.

View Article Online
DOI: 10.1039/D0CP03902K

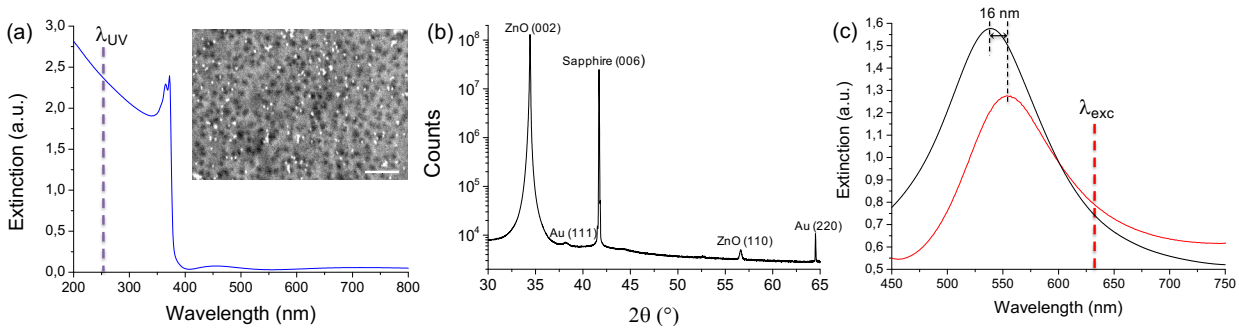

Fig. 1 (a) Extinction spectrum of the ZnO film of a 200-*nm* thickness (irradiation wavelength (λ_{UV}) is indicated in purple dashed line), and the inset displays a SEM picture of Au nanoparticles on the highly crystalline ZnO film (scale bar = 500 *nm*). (b) X-ray diffraction pattern of highly crystalline ZnO film decorated with AuNPs on sapphire substrate. (c) Extinction spectra of AuNPs on highly crystalline ZnO film before (in red) and after UV-irradiation taken 10 min after the stop of this irradiation (in black). The excitation wavelength (λ_{exc}) for Raman measurements is indicated in red dashed line.

crystalline ZnO film ($\lambda_{plasmon} = 555\ nm$) is far from the excitation wavelength for PIERS/SERS measurements ($\lambda_{exc} = 633\ nm$, see figure 1) inducing a very weak SERS signal. This novel type of substrate can be applied to a great number of plasmonic SERS nanostructures more complex than plasmonic nanospheres. For our investigation, the 200 *nm*-thick (highly crystalline) ZnO film was grown on sapphire (c-Al_2O_3) substrate by pulsed laser deposition. From the extinction spectrum of this ZnO film in figure 1a, a strong absorption is observed in UV region (200–380 *nm*). All the extinction spectra were recorded with a Cary-5000 spectrophotometer (Agilent) in transmission configuration. Then, gold nanoparticles (AuNPs) with a diameter of 30 *nm* were drop casted on the ZnO film and air dried (see Fig.1a and SI1, ESI†)). X-ray diffraction (XRD) pattern displayed in figure 1b shows a very intense and sharp diffraction peak for the (002) plane and a weak diffraction peak for the (110) plane of ZnO (wurtzite) indicating a high degree of crystallinity. Furthermore, another dominant diffraction peak is observed corresponding to the (006) plane of sapphire (c-Al_20_3) substrate, and weak diffraction peaks are also observed corresponding to the (111) and (220) planes of gold. Then, the AuNPs/ZnO film was irradiated by an UV lamp ($\lambda_{UV} = 254\ nm$) for 30 min. An extinction spectrum was recorded 10 min after the end of this UV irradiation as well as before the UV irradiation (see Fig.1c). A spectral blue-shift of 16 *nm* in the plasmon resonance (LSPR) of AuNPs was observed due to increasing electron density which can be estimated with the following expression determined in the work of Mulvaney *et al.* [21]:

$$\frac{\Delta N}{N} = \frac{-2\Delta\lambda}{\lambda_{plasmon}} \quad (1)$$

where $\Delta\lambda$ corresponds to the plasmon resonance shift and $\lambda_{plasmon}$ is the plasmon resonance position before UV irradiation ($\lambda_{plasmon} = 555\ nm$). Thus, we found $\Delta N/N = 5.8\%$. Moreover, the full width at half-maximum of the plasmon is also increased. Thus, the measurements confirmed a charge transfer mechanism from ZnO film to AuNPs, which is in agreement with previous works [15,22]. In addition, the plasmon resonance position of AuNPs in solution did not change when these latter were irradiated by UV lamp (see SI2, ESI†). For the study concerning the PIERS effect, the AuNPs were functionalized with thiophenol molecules (the used thiophenol concentration is 1 μM, see ESI†). The thiophenol molecule was chosen, because it is a small molecule whose the Raman signature is well-known. All the Raman spectra were recorded with a Labram spectrophotometer of Horiba Scientific with a spectral resolution of 1 cm^{-1} and an excitation wavelength of 633 *nm* (see ESI†). First, a SERS spectrum was recorded before UV-irradiation serving as reference. From this spectrum, four Raman peaks are observed at 999 cm^{-1}, 1022 cm^{-1}, 1073 cm^{-1} and 1573 cm^{-1} which are characteristic of the thiophenol molecule [23,24] (see Fig.2). These peaks respectively correspond to: C–H out-of-plane bending and ring out-of-plane deformation (called: γ(CH) and r–o–d); ring in-plane deformation and C–C symmetric stretching (called: r–i–d and ν(CC)); C–C symmetric stretching and C–S stretching (called: ν(CC) and ν(CS), respectively), and the C–C symmetric stretching mode (called: ν(CC)). In the SERS spectrum (see the red spectrum in Fig.2a), we observed weak SERS intensities for each Raman peak indicating that the electromagnetic contribution is very weak. Moreover, the SERS spectrum of AuNPs on sapphire substrate (without ZnO film) has also displayed weak SERS intensities for the Raman peaks, which has confirmed the very weak electromagnetic contribution (see SI3, ESI†). In addition, no signal enhancement was observed for the ZnO film with thiophenol (without AuNPs) before and after UV irradiation (see SI4, ESI†). Hereafter, by steps of 5 min, the sample is irradiated with the UV lamp (located at 2.4 cm above sample) followed by Raman measurement during which the UV lamp is switched off. We repeated this for each step of 5 min up to 30 min. During all these Raman measurements, the positions of the sample and the UV lamp were fixed, and during UV-irradiation, the laser source for Raman measurements ($\lambda_{exc} = 633\ nm$) is stopped by a shutter. Eventually, after the irradiation time of 30 min, the UV lamp is switched off in order to study the relaxation mechanism.

From Raman spectra recorded between 0 and 30 min, we observe an improvement of Raman signal that is due the PIERS effect (see Fig.2a). This latter is a charge transfer mechanism mediated by UV light from ZnO film to AuNPs. Indeed, oxygen vacancies (V_O) are created within ZnO film and their number increases over irradiation time. This generates electron donor

View Article Online
DOI: 10.1039/D0CP03902K

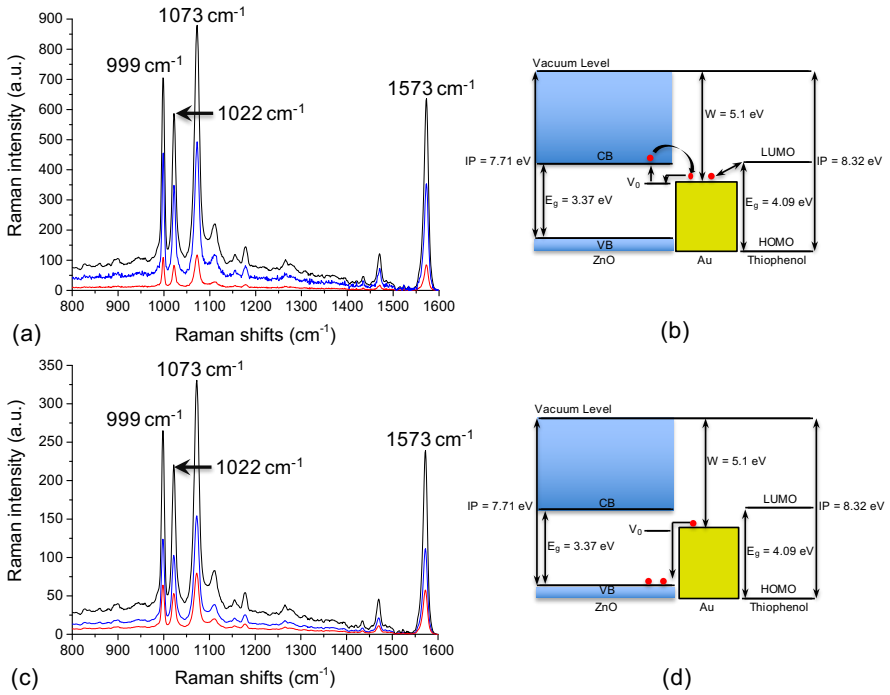

Fig. 2 (a) Raman spectra for an UV-irradiation time of 0 min (in red color, SERS spectrum serving as reference), 15 min (in blue color, PIERS spectrum), and 30 min (in black color, PIERS spectrum). (b) Principle scheme of PIERS mechanism. (c) Raman spectra for a relaxation time of 10 min (in black color), 20 min (in blue color), and 30 min (in red color) just after stopping UV irradiation. (d) Principle scheme of relaxation mechanism.

states at ∼0.9 eV below the ZnO conduction band edge[13]. Such a doping enables electrons to jump from V_O states to the conduction band of ZnO when the laser source of Raman is turned on, then to inject them into Au energy levels[15] (see Fig.2b). The injected charges shift the Fermi level of AuNP on broad apportionment of more negative values[15]. This broads the resonance conditions between the Fermi level of AuNP and the molecular orbitals of a wide number of molecules improving the probabilities of charge transfer transitions[15]. Here, a charge transfer mechanism from the Fermi level of AuNP to the lowest unoccupied molecular orbital (LUMO) level of thiophenol molecule (see Fig.2b) has occurred and enabled by the red laser (λ_{exc} = 633 *nm*; energy = 1.96 eV), thus enhancing the Raman signal (called charge-transfer resonance Raman enhancement)[25]. The ionization potentials are 7.71 eV[26] and 8.32 eV[27] for ZnO and thiophenol, respectively, and the gap energies associated to ZnO and thiophenol are 3.37 eV[13] and 4.09 eV[27], respectively. The work function (W) of gold is 5.1 eV[28]. Then, the Raman signal decreases down to normal Raman signal (SERS) when the UV irradiation is stopped (see Fig.2c). This relaxation mechanism is due to surface healing of ZnO film when the substrate is only exposed to air (see Fig.2d). Then, we defined the PIERS gain as follows:

$$G_{PIERS} = \frac{I_{PIERS}}{I_{SERS}} \qquad (2)$$

when I_{PIERS} corresponds to the Raman intensity with UV irradiation and I_{SERS} is the Raman intensity before UV irradiation (reference). We calculated this PIERS gain for the Raman shift at 1073 cm^{-1} of the thiophenol molecule, and observed the highest value of this gain was 7.52 ± 1.71 (see Fig.3, data in red). This value is well superior to this found for ZnO in reference[14] (G_{PIERS} = 3.16). Moreover, this value is also higher than those found for WO_3[14] and TiO_2 films[14,15] (G_{PIERS} = 5.11 and 3.07, respectively), and it is superior or similar to the values found for TiO_2 nanopores[16] (G_{PIERS} = 6.70–8.00) and diphenylalanine peptide nanotubes[17] (G_{PIERS} = 7.47–8.08). From figure 3, the LSPR blue-shift increased with the UV-irradiation time and decreased with the relaxation time. In fact, by using the expression (1), it was the electron density that increased or decreased. Thus, we observed that the G_{PIERS} increased with the electron density.

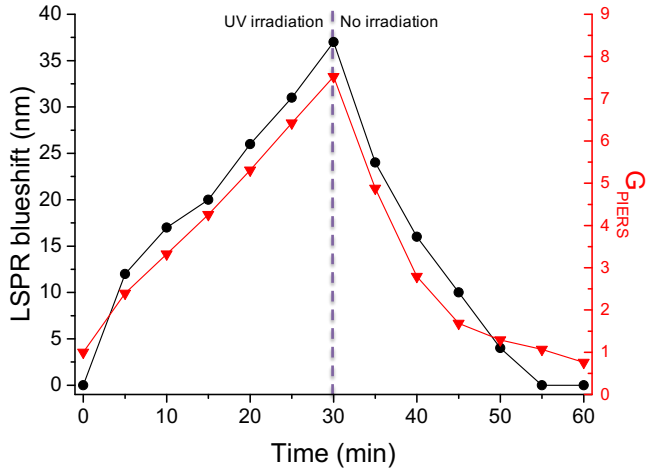

Fig. 3 The black points and red triangles correspond to LSPR blueshift of AuNPs, and PIERS gain (G_{PIERS}) as function of time, respectively. The purple dashed line corresponds to the stop of the UV irradiation.

View Article Online
DOI: 10.1039/D0CP03902K

Moreover, this higher value of the PIERS gain was due to a larger production of oxygen vacancies caused by the porous structure of our ZnO film compared to the smooth structure of ZnO film observed in reference [14], which is reported for decreasing the vacancy production [14]. In addition, we observed weak fluctuations of this Raman signal (see Fig.4) with relative standard deviations (RSDs) inferior to 14% compared to those observed for a weakly crystalline ZnO film [14], stating the very good uniformity of the PIERS signal of our sample. We attributed these lower fluctuations of Raman signal to the high crystallinity of ZnO film.

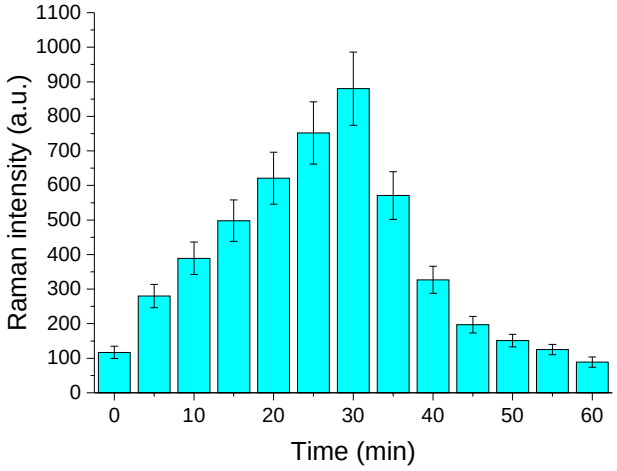

Fig. 4 Raman intensity as function of time for the Raman peak of thiophenol at 1073 cm^{-1}.

In summary, we demonstrated the easy manufacturing of a highly crystalline ZnO film decorated with Au nanoparticles which provides an efficient PIERS effect. We measured its performance at an excitation wavelength of 633 *nm* in order to only study the PIERS effect (chemical enhancement) based on charge transfer mechanisms between ZnO film and molecules via gold nanoparticles. This led to weaker fluctuations of PIERS signal (RSD < 14%) compared to the work of Glass *et al.* concerning to a weakly crystalline ZnO film [14]. We can explain these weaker fluctuations by the higher crystallinity of ZnO film. The highest PIERS gain was 7.52 which is well superior or similar to those obtained in current literature. The PIERS effect can be employed for improving Raman signals of a great number of biomolecules for applications to environmental protection and biological analysis.

Conflicts of interest

There are no conflicts to declare.

Notes and references

1 S. Kasera, *et al.*, Quantitative multiplexing with nano-self-assemblies in SERS, *Sci. Rep.*, 2014, **4**, 6785.

2 J. F. Bryche, *et al.*, Low-cost SERS substrates composed of hybrid nanoskittles for a highly sensitive sensing of chemical molecules, *Sens. Actuators B*, 2017, **239**, 795–799.

3 W. Ye, *et al.*, CTAB Stabilizes Silver on Gold Nanorods, *Chem. Mater.*, 2020, **32**, 1650–1656.

4 G. Gonzalez-Rubio, *et al.*, Surfactant-Assisted Symmetry Breaking in Colloidal Gold Nanocrystal Growth, *ChemNanoMat*, 2020, **6**, 698–707.

5 J. Henzie, *et al.*, Nanofabrication of Plasmonic Structures, *Annu. Rev. Phys. Chem.*, 2009, **60**, 147–165.

6 A. Dhawan, *et al.*, Deep UV nano-microstructuring of substrates for surface plasmon resonance imaging, *Nanotechnology*, 2011, **22**, 165301.

7 M. Bechelany, *et al.*, Simple Synthetic Route for SERS-Active Gold Nanoparticles Substrate with Controlled Shape and Organization, *Langmuir*, 2010, **26**, 14364–14371.

8 J. F. Bryche, *et al.*, Surface enhanced Raman scattering improvement of gold triangular nanoprisms by a gold reflective underlayer for chemical sensing, *Sens. Actuators B*, 2016, **228**, 31–35.

9 T. Ding, *et al.*, Nanoimprint lithography of Al Nanovoids for Deep-UV SERS, *ACS Appl. Mater. Interfaces*, 2014, **6**, 17358–17363.

10 S. Y. Ding, *et al.*, Electromagnetic theories of surface-enhanced Raman spectroscopy, *Chem. Soc. Rev.*, 2017, **46**, 4042–4076.

11 M. Fernanda Cardinal, *et al.*, Expanding applications of SERS through versatile nanomaterials engineering, *Chem. Soc. Rev.*, 2017, **46**, 3886–3903.

12 I. Alessandri, J. R. Lombardi, Enhanced Raman Scattering with Dielectrics, *Chem. Rev.*, 2016, **116**, 14921–14981.

13 S. B. Zhang, *et al.*, Intrinsic n-type versus p-type doping asymmetry and the defect physics of ZnO, *Phys. Rev. B*, 2001, **63**, 075205.

14 D. Glass, *et al.*, Dynamics of Photo-Induced Surface Oxygen Vacancies in Metal-Oxide Semiconductors Studied Under Ambient Conditions, *Adv. Sci.*, 2019, **6**, 1901841.

15 S. Ben-Jaber, *et al.*, Photo-induced enhanced Raman spectroscopy for universal ultra-trace detection of explosives, pollutants and biomolecules, *Nat. Commun.*, 2016, **7**, 12189.

16 M. Zhang, *et al.*, Three-Dimensional TiO_2–Ag Nanopore arrays for Powerful Photoinduced Enhanced Raman Spectroscopy (PIERS) and Versatile Detection of Toxic Organics, *ChemNanoMat*, 2019, **5**, 55–60.

17 S. Almohammed, *et al.*, Photo-induced surface-enhanced Raman spectroscopy from a diphenylalanine peptide nanotube-metal nanoparticle templates, *Sci. Rep.*, 2018, **8**, 3880.

18 T. Jiang, *et al.*, *In situ* controlled sputtering deposition of gold nanoparticles on MnO_2 nanorods as surface-enhanced Raman scattering substrates for molecular detection, *Dalton Trans.*, 2015, **44**, 7606–7612.

19 Y. Chen, *et al.*, In Situ Recyclable Surface-Enhanced Raman Scattering-Based Detection of Multicomponent Pesticide Residues on Fruits and Vegetables by the Flower-like MoS_2@Ag Hybrid Substrate, *ACS Appl. Mater. Interfaces*, 2020, **12**, 14386–14399.

View Article Online
DOI: 10.1039/D0CP03902K

20 A. Fularz, *et al.*, Oxygen Incorporation-Induced SERS Enhancement in Silver Nanoparticle-Decorated ZnO Nanowires, *ACS Appl. Nano Mater.*, 2020, **3**, 1666–1673.

21 P. Mulvaney, *et al.*, Drastic Surface Plasmon Mode Shifts in Gold Nanorods Due to Electron Charging, *Plasmonics*, 2006, **1**, 61–66.

22 A. M. Brown, *et al.*, Electrochemical tuning of the dielectric function of Au nanoparticles, *ACS Photonics*, 2015, **2**, 459–464.

23 C. G. Tetsassi Feugmo, V. Liegeois, Analyzing the vibrational signatures of thiophenol adsorbed on small gold clusters by DFT calculations, *ChemPhysChem*, 2013, **14**, 1663–1645.

24 S. Lis, *et al.*, Theoretical and experimental studies on the adsorption behavior of thiophenol on gold nanoparticles, *J. Raman Spectrosc.*, 2007, **38**, 1436–1443.

25 L. Jensen, C. M. Aikens, G. C. Schatz, Electronic structure methods for studying surface-enhanced Raman scattering, *Chem. Soc. Rev.*, 2008, **37**, 1061–1073.

26 A. Walsh, K. T. Butler, Prediction of Electron Energies in Metal Oxides, *Acc. Chem. Res.*, 2014, **47**, 364–372.

27 M. R. Gartia, *et al.*, Metal–Molecule Schottky Junction Effects in Surface Enhanced Raman Scattering, *J. Phys. Chem. A*, 2011, **115**, 318–328.

28 X. Zhang, *et al.*, Plasmonic photocatalysis, *Rep. Prog. Phys.*, 2013, **76**, 046401.